Hydrology Research

Hydrology Research Vol 55 No 1, 67 doi: 10.2166/nh.2023.146

The Next-Generation Ecosystem Experiment Arctic Rainfall Simulator: a tool to understand the effects of changing rainfall patterns in the Arctic

Caleb Renner[a], Nathan Conroy[a], Evan Thaler[a,*], Adam Collins[a], Lauren Thomas[a], Shannon Dillard[a,b], Joel Rowland[a] and Katrina Bennett[a]

[a] Division of Earth and Environmental Science, Los Alamos National Laboratory, Los Alamos, New Mexico, USA
[b] Department of Geography, University of Wisconsin – Madison, Madison, Wisconsin, USA
*Corresponding author. E-mail: thaler@lanl.gov

ET, 0000-0002-4408-9321

ABSTRACT

Rainfall frequency and intensity are expected to increase in the Arctic, with potential detrimental impacts on permafrost, leading to enhanced thawing and carbon release to the atmosphere. However, there have been very few studies on the effect of discrete rain events on permafrost in the Arctic and sub-Arctic. Conducting controlled rainfall experiments within permafrost landscapes can provide an improved understanding of the effect of changing intensity, duration, and timing of rain events on permafrost tundra ecosystems. Here, we describe the design and implementation of the Next-Generation Ecosystem Experiment Arctic Rainfall Simulator (NARS), a variable intensity (4–82 mm/h) rainfall simulator that can be used to study the effects of rainfall on permafrost stability. The NARS design includes a 3D-printed 4 cm H-flume and uses an eTape resistivity sensor that was calibrated ($R^2 = 0.9$–0.96) to measure discharge from the system. NARS is designed to be lightweight, simple to construct, and can be easily deployed in remote locations. As a field validation of updated rainfall simulator design and modernized controls, NARS was tested on the Seward Peninsula, AK. Because of its portability, versatility in deployment, dimensions, and rainfall intensity, NARS represents a methodological innovation for researching the impacts of rainfall on permafrost environments.

Key words: Arctic, field experimental design, permafrost, permafrost thaw, rainfall, rainfall simulator

HIGHLIGHTS

- Rainfall is expected to increase in the Arctic over the next century.
- The effects of rainfall on permafrost stability are poorly understood.
- We developed a variable intensity rainfall simulator for use in remote areas.
- The new rainfall simulator is lightweight and modernizes simulator controls.
- The simulator can be used to study rain effects on permafrost.

GRAPHICAL ABSTRACT

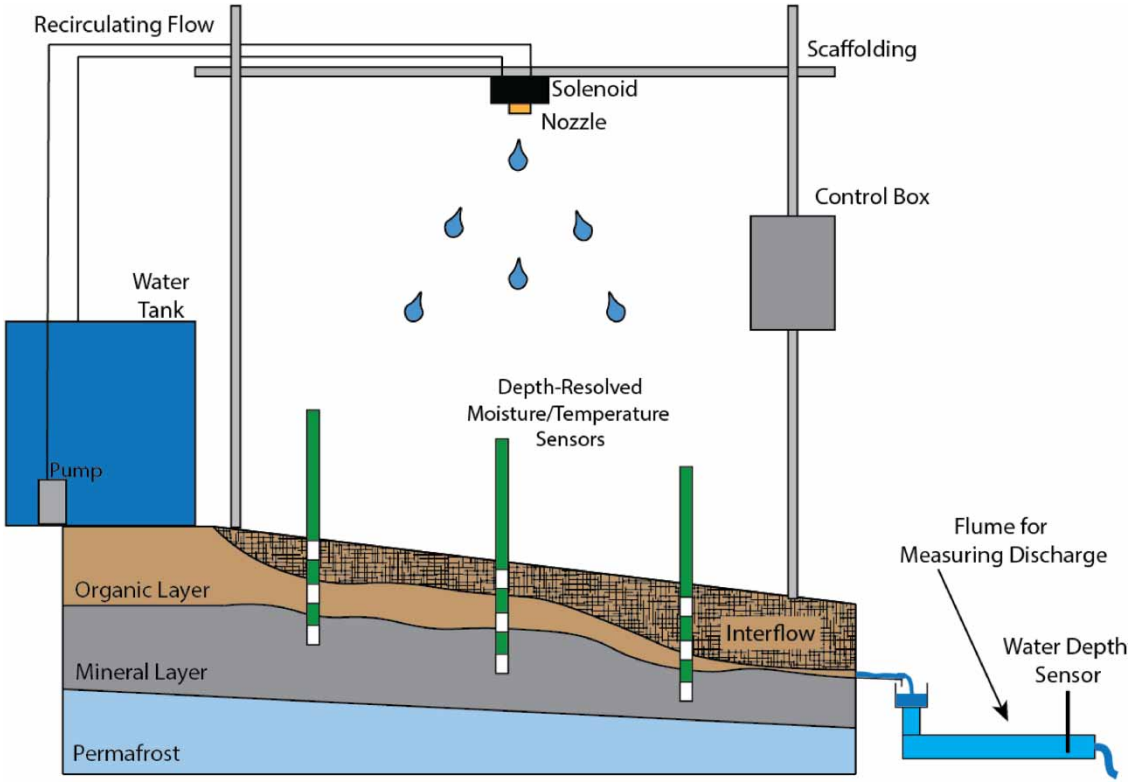

1. INTRODUCTION

Permafrost, defined as ground that remains at or below 0 °C for at least 2 consecutive years, underlies ~15% of the exposed land surface area of the Northern Hemisphere (Obu 2021). Because permafrost soils store vast amounts of carbon, they are a critical component of the global carbon cycle (Olefeldt *et al.* 2016; Lindgren *et al.* 2018), and thawing of these soils can cause the release of an unknown magnitude of carbon to the atmosphere (Schuur *et al.* 2015; Miner *et al.* 2022). Permafrost soils are also important on regional and local scales because they regulate the hydrologic flux from uplands to rivers and oceans (Lafrenière & Lamoureux 2019). Thawing of permafrost soils can increase the hydrologic connectivity between hillslopes and rivers in Arctic landscapes, resulting in increased solute and nutrient fluxes to rivers (Bowden *et al.* 2008; Lafrenière & Lamoureux 2019).

The vulnerability of permafrost soils to warming climatic conditions is strongly influenced by the dynamic ecosystem structure (Jorgenson *et al.* 2010) and precipitation type, extent, and duration (Douglas *et al.* 2020). The magnitude of precipitation in the Arctic is expected to increase by 60% (Bintanja & Selten 2014), and the proportion of precipitation falling as snow relative to rain is predicted to decrease by up to 40% by the year 2100 (McCrystall *et al.* 2021). Although the effect of snow on the permafrost thermal regime is well documented through numerous field, experimental, and modeling studies (e.g., Sturm *et al.* 2001; Myers-Smith & Hik 2013; Grünberg *et al.* 2020; Domine *et al.* 2022), few observational studies (e.g., Iijima *et al.* 2010; Douglas *et al.* 2020) and fewer field experiments (e.g., Magnússon *et al.* 2022) have assessed the impact of rainfall timing, duration, and magnitude on permafrost stability within Arctic landscapes.

Rainfall simulators (RFSs) are tools used to study the effects of rainfall on various processes at the plot scale. RFSs enable controlled and repeatable experiments to be conducted over instrumented plots without the spatial and temporal limitations of natural rainfall and can also be used to study storms with low recurrence intervals. They are capable of producing rainfall with similar intensity, uniformity, and raindrop characteristics as natural rain (Meyer & Harmon 1979; Agassi & Bradford 1999; Humphry *et al.* 2002; Paige *et al.* 2004) by using agricultural spray nozzles and conduit supported by a scaffolding system (Tossell *et al.* 1987; Agassi & Bradford 1999; Humphry *et al.* 2002; Polyakov *et al.* 2018).

RFSs have been used since the 1940s to study the effects of rainfall on plot-scale hydrology and erosion (Beutner *et al.* 1940; Free *et al.* 1940) and to inform and validate process-based models (e.g., Schindewolf & Schmidt 2012; Schoener & Stone 2019). In addition, RFSs have been used to study the impacts of fire (Pierson *et al.* 2009), vegetation type and cover (Quinton *et al.* 1997), the effect of antecedent moisture conditions on runoff and erosion (Schoener & Stone 2019), transportation of chemicals through runoff and interflow (Singh *et al.* 2000), and the alteration of surface roughness by rainfall (Li *et al.* 2020). RFSs have primarily been deployed in arid environments and agricultural settings (e.g., Tossell *et al.* 1987; Pierson *et al.* 2009; Schoener & Stone 2019), often locations that can be accessed using vehicles, minimizing logistical concerns for deployment such as RFS weight and water supply.

RFS design can be broadly defined into two categories: (1) fixed nozzle simulators and (2) rotating boom simulators. Fixed nozzle simulators (e.g., Humphry *et al.* 2002) use a fixed nozzle pointing downward that produces a round or square full cone spray pattern to produce even rainfall over the plot area (Tossell *et al.* 1987; Humphry *et al.* 2002). They are simple to deploy and do not require any external computer control. However, fixed nozzle simulators are limited by the ability to produce only one rainfall intensity for a given nozzle and water pressure (Tossell *et al.* 1987; Agassi & Bradford 1999; Humphry *et al.* 2002). On the other hand, rotating boom simulators (e.g. Walnut Gulch Rainfall Simulator) have the capability of producing multiple rain intensities using the same nozzles and water pressure; rain intensity is controlled by the rate of boom rotation and the time that nozzles are discharging to the plot (Agassi & Bradford 1999; Paige *et al.* 2004). However, rotating boom simulators are more complicated than fixed nozzle simulators, requiring a motor to rotate the boom, solenoids to control water discharge, and electronics to control hardware, and are therefore more difficult to deploy in isolated locations.

There is a dearth of *in situ* rainfall experiments in the Arctic. Indeed to date, only one other study has used an RFS to study the effects of rainfall on permafrost stability dynamics in Sibera (Magnússon *et al.* 2022); however, the RFS used in that study was limited by its ability to change the rainfall application rate. The lack of other experimental rainfall studies in the Arctic is due in part to the lack of a suitable RFS design; deployment in remote Arctic environments requires a lighter, simpler, and modernized RFS that can produce variable rainfall intensity while capturing runoff data. Here, we document the design and implementation of a variable application rate RFS for the Arctic, which was developed for the Department of Energy Next-Generation Ecosystem Experiments (NGEE) Arctic project, and hence, we name the design the NGEE Arctic Rainfall Simulator (NARS). NARS is a tool for studying the effects that more frequent and intense rainfall will have on permafrost environments in the changing Arctic.

2. METHODS

2.1. The NGEE Arctic rainfall simulator overview

The NARS is a variable intensity RFS with design aspects based on the study by Humphry *et al.* (2002) and the Walnut Gulch (Paige *et al.* 2004) RFSs. NARS uses an aluminum frame that can be fully deconstructed for transportation to field sites, and a water recycling system that enables variable rainfall intensity. Rain intensity control and data logging are automated with a Raspberry Pi (RPi) microcomputer (Model 4B, Raspberry Pi Ltd, Pencoed, Wales, UK). Water temperature is measured before the nozzles using a type K thermocouple, and discharge is measured using a specially developed 3D-printed micro-HS-flume and eTape® Liquid Level Sensor (12110215TC-5, Milone Technologies, Sewell, NJ, USA) using the RPi. The equipment and parts required to build NARS were obtained from readily available commercial retail sources at a cost of approximately $10,000 USD as of February 2022.

2.1.1. Scaffolding frame

NARS uses a modular frame design based on Humphry *et al.*'s (2002) RFS frame (Figure 1(a)). Each cuboid frame module has a 1.5 m × 2 m rectangular footprint resulting in a 1.45 m × 1.9 m rain plot. Individual frame modules can be merged to produce a larger experimental plot. The frame is constructed with 25 mm IPS aluminum pipe (1' Iron Pipe Size) and Hollaender® Speed-Rail® adjustable fittings (Cincinnati, OH, USA, Figure 1(b)) that are numbered to ensure proper orientation for construction. The pins on the fittings were replaced with wire-locking clevis pins (98416A211, McMaster-Carr®), which facilitate rapid assembly with minimum tools in approximately 30 min in optimal conditions. One individual frame module weighs ~27 kg and can be fully deconstructed and bundled together for transportation to field locations. Adjustable legs enable the simulator frame to be leveled over field plots on slopes up to ~17°. Once constructed, the frame is rigid and light enough to be transported short distances by a recommended minimum of four people.

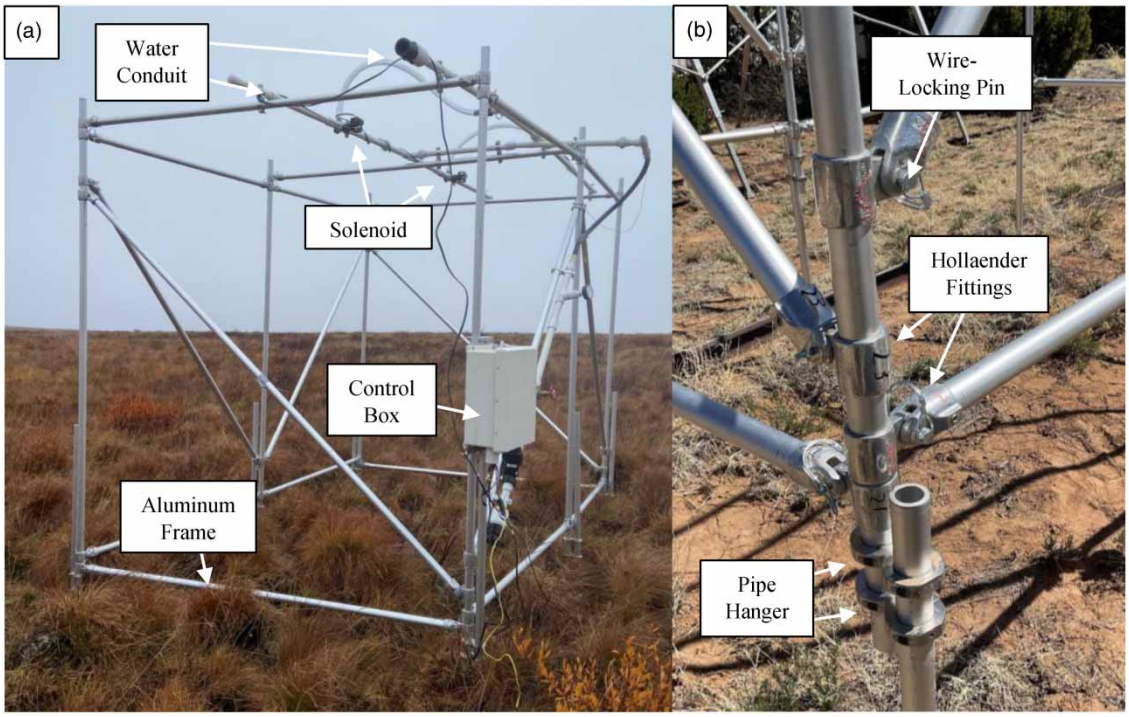

Figure 1 | The NARS with major components highlighted. (a) NARS is a variable intensity rainfall simulator specially designed for deployment in remote Arctic environments. The aluminum frame supports water conduit constructed with 25 mm PVC pipe, and the control box can be attached to the simulator using U-Bolts. (b) NARS uses a 25 mm aluminum pipe frame that is joined together using Hollaender fittings secured with wire-locking pins, facilitating rapid construction without needing tools. The NARS is leveled over the rainfall plot by adjusting the legs that are connected to the main frame with stackable pipe hangers.

To minimize wind and rain effects during a simulation, polyethylene tarps with 10 mil thickness are fixed to the sides and top of the simulator frame using 28 cm tarp bungee cords (Supplementary Figure S1). For accurate rainfall application, water dripping from the frame and surrounding tarps must not hit the plot, which can be accomplished through accurately positioning the simulator over the plot, staking the tarps down away from the plot, and using a guttering system to direct any errant drips away.

2.1.2. Water system

Like the Walnut Gulch design (Paige *et al.* 2004), NARS uses a water recycling system that eliminates pressure spikes as the solenoids actuate and reduces water use (Figure 2). Water is constantly circulated between the simulator and the water tank using a series of hoses and pipes to maintain stable system pressure. Water is directed either onto the plot or into the return line using solenoid valves.

NARS uses two AA144A DirectoValve® three-way solenoid valves (TeeJet®, Glendale Heights, IL, USA) that are centered in each module. Using solenoid valves allows for prompt changes in rainfall intensity by changing the time that the plot-facing nozzle is active without changing nozzles or water pressure. FullJet® ½-HH50-WSQ (Spraying Systems Co.®, Glendale Heights, IL, USA) nozzles are used for the two solenoid outlets to maintain constant water pressure; one outlet is directed to the plot, and the other is directed to the water return line. The FullJet nozzle was selected for its square-shaped, uniform spray pattern and the ability to produce raindrops with characteristics comparable to natural rainfall (i.e., rain drop size distribution and kinetic energy) (Humphry *et al.* 2002).

NARS water conduit is constructed from 25 mm IPS PVC pipe that is 3 m long when constructed. For ease of transportation, it can be separated into 1 m sections that are joined using threaded PVC unions. The conduit is fastened to the frame with pipe hangers (Figure 1(a)), enabling the simulator to be disassembled efficiently for shipping to the field or transporting in a vehicle. Rather than using rigid agricultural water tanks to store and supply water for rainfall experiments, water is stored in portable vinyl tanks (Husky® Portable Containment, Bartlesville, OK, USA) that weigh 18 kg and can be carried

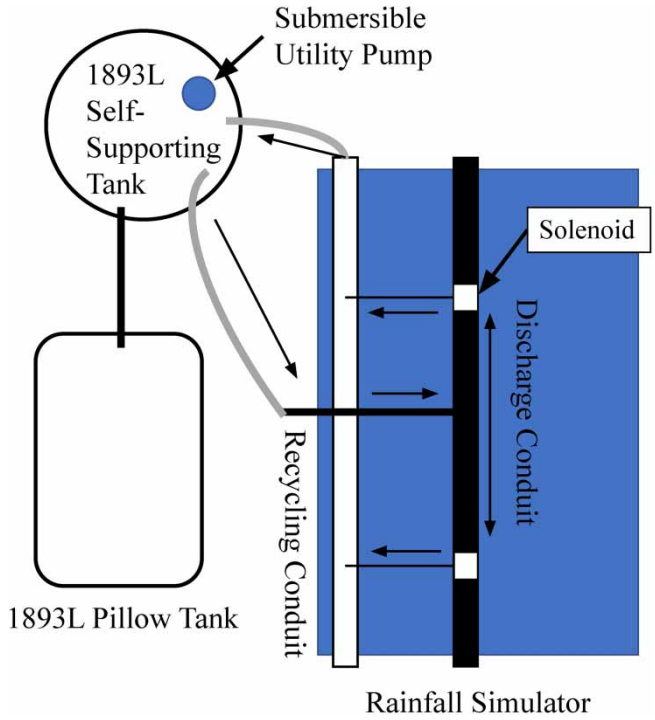

Figure 2 | Schematic diagram of the water recycling system with arrows showing water flow path. Water is pumped from the self-supporting water tank to the discharge conduit using garden hoses, where water is either directed to the plot or recycling conduit via a solenoid valve. A spray nozzle is plumbed into both solenoid outlets. Water flows from the recycling conduit back into the self-supporting tank. This system maintains a continuous water pressure regardless of which direction the solenoid is open to and reduces water usage.

to the field location by hand. A 1,893 L self-supporting water tank was used to supply water directly for the RFS experiments, and a 1,893 L auxiliary pillow tank stored additional water nearby (Supplementary Figure S2).

2.1.3. NARS control

NARS is controlled with an RPi microcomputer (Supplementary Figure S3). Unlike other simulators that require a computer separate from an external data logger, a single RPi can be programmed to simultaneously control rainfall intensity and collect data from a variety of sensors including water temperature and flume water depth instruments.

The RPi interfaces with different instruments to control rainfall intensity, measure applied rainfall temperature, and measure rainwater runoff from the plot. Rainfall intensity is moderated through the time solenoid valves spray water onto the plot. The timing is automated through a relay signal, which opens and closes the solenoids in a 10 s loop controlled by the RPi. While drop size distribution and kinetic energy of natural rain are variable as intensity changes (Agassi & Bradford 1999), water discharged by NARS has only one rate, it is either fully on or fully off, and the drop size distribution and kinetic energy remain the same throughout the simulation. However, to achieve different rain characteristics, different nozzles could be selected.

The applied rainfall temperature was measured using a K type thermocouple (1245N15, McMaster-Carr), which was selected for its simplicity in integrating with the RPi. Measuring the water temperature prior to application allows users to account for thermal impacts of rainfall within the RFS plot.

A Milone eTape® Liquid Level Sensor (eTape), a variable resistor where resistance changes corresponding to submersion depth, was selected to measure water depth in the discharge flumes (described in section 2.1.4). An Arduino Uno (Rev3, Scarmagno, Italy) microcontroller converted the eTape's analog measurements into a digital signal that can then be read by the RPi. To ensure accurate measurements, bending of the sensor was prevented by installing the eTape adjacent to the main flume channel in a stilling well with a diameter equal to its width.

A graphical user interface (GUI) application was developed to automate NARS control and make it user friendly (Supplementary Figure S4) and can be found at https://doi.org/10.5440/1960551. The GUI enables data processing to perform

in the background, so users do not need to be familiar with programming to control NARS. The GUI consists of a slider that controls the rain intensity and buttons to start and stop data acquisition. The slider has 20 settings that correspond to rain intensity from 4 to 82 mm/h and rain intensity can be adjusted during an experiment by adjusting the slider setting. There are also individual buttons to control data acquisition for the thermocouple and the flume. As data are collected, real-time measurements from the instruments are displayed on the screen so that anomalies can be immediately addressed. Data collected by the sensors are automatically saved to a file during each loop. If the RPi were to fail, rain intensity can be controlled using a toggle switch where the user manually opens and closes the solenoid circuit in a timed sequence, which actuates the solenoid valves, to achieve a variable rain intensity.

2.1.4. Discharge measurements

Discharge was measured using an H-flume (Figure 3). The H-flumes can measure a wide range of flows and offer better low flow sensitivity while maintaining high flow capacity (Brakensiek *et al.* 1979). They have a flat floor, which enable sediment and other solids to pass through, though smaller H-flumes are limited in the size of material that can pass through. To ensure accurate discharge measurements, H-flumes must be level in all directions and drain freely (Brakensiek *et al.* 1979).

There are three classes of H-flumes: HS (small), H (standard), and HL (large), which have standardized dimensions that are based on the height (h) of the flume (Gwinn & Parsons 1976). HS-flumes are the narrowest, and the smallest HS-flume (12.2 cm) can measure flows from 4.5 to 2,274 mL/s (Brakensiek *et al.* 1979). HS-flumes have a total length of 1.5 h, a width of 1.05 h, and an outlet width of 0.5 h, and the measurement point is h length from the outlet (Brakensiek *et al.* 1979). To ensure laminar flow of the fluid entering the flume, a rectangular approach length of 3–5 h is installed ahead of flume (Gwinn 1984; Marr *et al.* 2010).

The smallest commercially available flumes lacked the flow sensitivity required for the low discharge rates expected from NARS experiments. Running NARS at full intensity produces rainfall at 82 mm/h over the 2.9 m $\times$ 1.9 m rectangular plot,

Figure 3 | The flume system consists of angle iron, PVC guttering, and 3D-printed 4 cm micro-HS-flume. The 4 cm micro-HS-flume has a total length of 27 cm. Water from the RFS plot is captured by the angle iron, which is hammered in parallel to the slope, so that runoff can be measured. Water drains from the lip of the angle iron into a PVC guttering system constructed out of 50 mm IPS PVC pipe cut in half and a 50–25 mm IPS PVC reducing tee. Water leakage is mitigated by using plumbing putty to seal joints. Water then flows into the 3D-printed 4 cm micro-HS-flume that has been calibrated to the recorded eTape resistance. A waterproof box contains an Arduino, which converts the analog resistance signal to a digital signal that can be recorded by the Raspberry Pi.

and, assuming all water runs off from the plot, the maximum expected discharge would only be 122 mL/s. Although some of our Arctic study sites during frozen conditions might produce the maximum discharge, we required, and designed, a 'Micro'-HS-flume that had even lower flow response to measure the expected discharge range produced by NARS. The micro-HS-flume dimensions were based on scaling the standardized HS-flume dimensions. The height was 4 cm, giving the flume a length of 6.1 cm, a width of 4.25 cm, an outlet of 0.2 cm, and an approach length of 20 cm. A stilling well with an inner diameter of 2.66 cm was installed at the measurement point to hold the eTape. For this work, two 3D-printed micro-HS-flumes were designed, one with a 0.64 cm × 0.64 cm opening to the stilling well and the other with a 1 cm × 3.6 cm opening.

The 4 cm micro-HS-flumes were 3D printed because there are no commercially available H-flumes with these dimensions. 3D printing is an inexpensive way to produce flumes while still providing consistent flow measurements, making them suitable for hydrologic monitoring (Akhter *et al.* 2021). The micro-HS-flume was printed using 1.75 mm Tough PLA plastic filament (MatterHackers Lot #24370, Lake Forest, CA, USA) using a 0.6 mm nozzle installed on a Prusa i3 MK3 3D printer (Prusa Research, Prague, Czech Republic) and sliced using PrusaSlicer software. Nozzle temperature was held at 220 °C throughout the print and bed temperature was held at 65 °C for the first layer and 60 °C for all subsequent layers. The lightning infill pattern was used with a fill density of 15%. The flume and the stilling well were printed separately and glued with silicon glue after printing. Overall, each flume print consumed approximately 240 g of PLA filament and required ~16.5 h to print.

2.2. Validation

2.2.1. NARS intensity and uniformity

NARS rainfall intensity and uniformity validation experiments were conducted after the procedures described in studies by Humphry *et al.* (2002) and Tossell *et al.* (1987), positioning the nozzles in different configurations to investigate contributions of spacing and height on rainfall patterns.

Intensity and uniformity were measured by regularly distributing 48 Petri dishes in an 8 × 6 grid over the 1.9 m × 1.45 m rectangular rainfall plot for single-frame module experiments and 96 Petri dishes in an 8 × 12 grid over the 1.9 m × 2.9 m rectangular rainfall plot for double-frame module experiments. The single-frame module setup used a single nozzle centered over the plot; the double-frame module setup used two nozzles that were spaced equal distances from the center of the simulator frame. Each nozzle was spaced 71.1 cm from the center of the simulator, centering each nozzle in their respective frame module. To test the effect of nozzle spacing on uniformity, the spacing was increased to 101.6 cm from the center and again to 127 cm from the center of the simulator. The nozzle height was reduced from 3 to 2.4 m to evaluate the effect of simulator height on uniformity.

NARS was run with continuous rainfall for 1.5 min, and then the water volume in each dish was measured. Intensity was calculated following Equation (1):

$$I_P = 10\left[\frac{\left(\sum_{i=1}^{n}\frac{V_i}{A_g}\right)}{n} \times \frac{60}{t}\right] \tag{1}$$

where I_P is the average intensity in mm/h; V_i is the volume of the ith Petri dish in cm^3; A_g is the Petri dish surface area in cm^2; n is the number of Petri dishes; t is the time of each run in minutes; and the coefficient of 10 converts measurements from cm/h to mm/h (Tossell *et al.* 1987).

The measured volume in each dish was used to calculate the uniformity coefficient (Christiansen 1940):

$$\mathrm{UC} = 100\left(1.0 - \frac{\sum_{i=1}^{n}|X_i|}{mn}\right) \tag{2}$$

where UC is the uniformity coefficient as a percentage; X_i is the deviation from the mean; m is the mean volume of rainfall; and n is the number of gauges used (Tossell *et al.* 1987). If a Petri dish spilled during an experiment, the average volume of adjacent Petri dishes would be used in place of the errant volume of the spilled dish, which is a likely source for some error in the uniformity calculations; however, this uncertainty has not been quantified in this study.

2.2.2. eTape calibration and micro-HS-flume

The eTape selected for our application had a sensor length of 120 mm. To determine the activation depth (the minimum fluid depth necessary before sensor resistance changes with fluid depth) and sensitivity (the minimum detectable resistance change from changing fluid height) of the eTape, it was placed in a 250 mL graduated cylinder with a 33 mm inner diameter and was suspended from the bottom of the beaker by ~1 mm, while ensuring that the eTape was not bent. Tap water was pipetted into the graduated cylinder in 0.5–5 mL increments; each additional mL of water added corresponded to ~1 mm increase of visual water height on the eTape (Table 1). The visual eTape height, mass of water added, total water mass, and eTape resistance were recorded after each addition of water. Net eTape resistance was calculated by subtracting the measured resistance value from the resistance at zero water depth. Activation depth was determined from the minimum water depth before eTape resistance values changed, and sensitivity was determined by the minimum addition of water necessary to change the sensor resistance after the activation depth had been reached.

The eTape resistance was calibrated to the discharge of a commercially available 12.2 cm HS-flume and the 3D-printed 4 cm micro-HS-flumes. The flumes were leveled with the flume freely spilling into a sink, and the eTape was installed in each flume's stilling well. In the commercially available 12.2 cm HS-flume, which had a 101.6 mm diameter stilling well, the eTape was taped to the side to prevent the sensor from floating or shifting. The 4 cm micro-HS-flumes had a 2.54 cm diameter stilling well, which was narrow enough to support the eTape without any adhesives. The eTape was primed past the activation depth to a depth of 68 mm in the 12.2 cm HS-flume, which corresponded to the height where the top of the eTape was level with the top of the stilling well, and 28 mm in the 4 cm Micro-HS-Flumes. Tap water was run from the faucet through the flume. Water was collected from the flume using a 400 mL beaker, and discharge was calculated by timing the rate to fill the beaker with water. Discharge was increased in ~7 mL/s increments, limited by the coarseness in adjusting the faucet valve. The mass of water was measured and then converted to volume. Discharge in mL/s was calculated by dividing volume by time elapsed to reach that volume. Within this experiment, the timing rate, coarseness in discharge increment increases, and visual mistakes in reading the beaker lines are all sources of minor error.

2.2.3. Arctic field deployment

A five-person team deployed NARS in late September through early October 2022 to the Kougarok Fire Complex at the end of the Nome-Taylor Highway, Seward Peninsula, AK (Figure 4), as a proof-of-concept test of NARS operation in a sub-Arctic permafrost environment. Temperatures ranged from −4 to 4 °C with sunny to partly cloudy days. The RFS experimental plots were located in continuous permafrost with an average thaw depth of 57 cm on a northwest-facing hillslope to the southeast of Mauze Gulch, which drains to the Kougarok River. Experiments were conducted in burned tussock tundra (Liljedahl *et al.* 2007; Sulman *et al.* 2021).

Equipment was transported to a staging location 70 m from the RFS plots in the bed of two trucks and then hiked into the field location. To preserve the integrity of the study site, the frame was constructed 5 m from the RFS plots and was carried to

Table 1 | Water was added to the 250 mL beaker in 0.5–5 mL increments

Additional water (mL)	eTape visual height range
2	0–20
1	20–30
2	30–40
5	40–60
0.5	60–70
5	70–100
2.5	100–110
0.5	110–120

Note: This table shows how much water was added for a given visual height range on the eTape sensor.

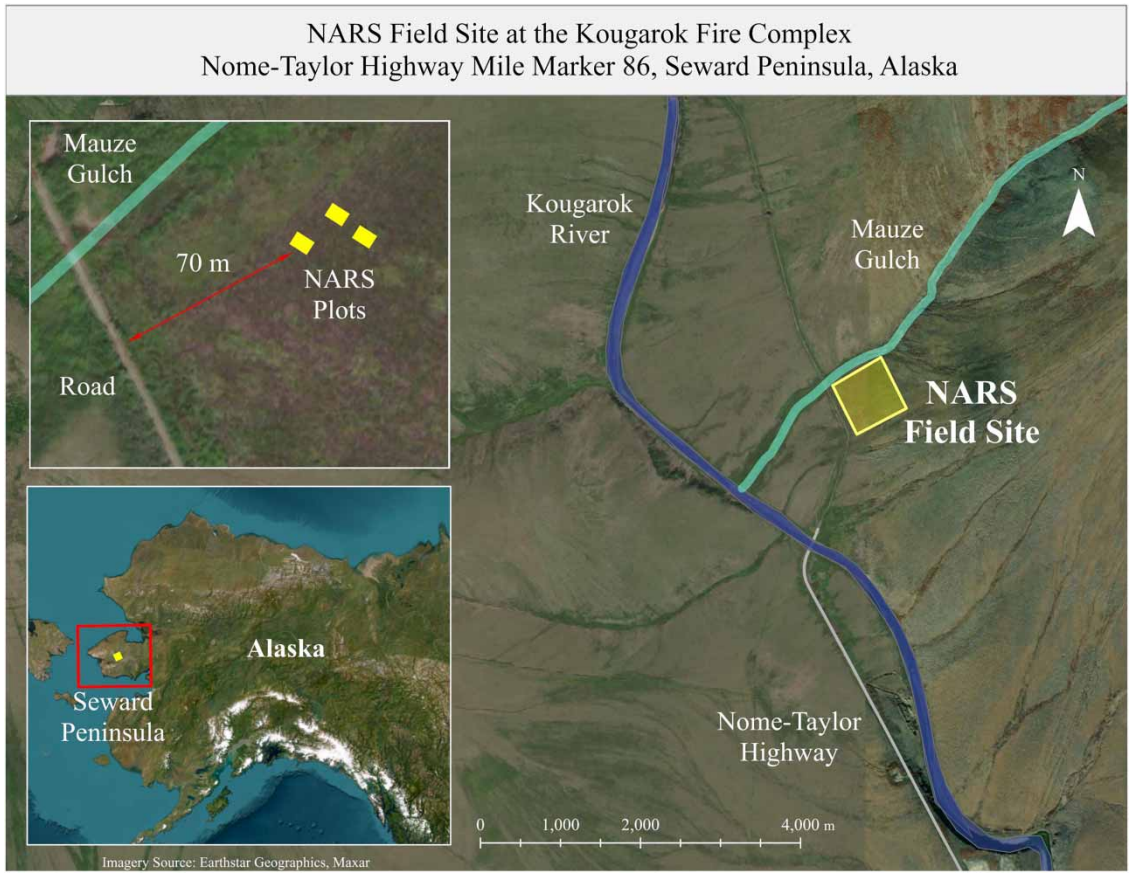

Figure 4 | Location of the field deployment site on the Seward Peninsula in Western Alaska. The NARS rainfall simulation experiments were carried out at the Kougarok Fire Complex at the end of the Nome-Taylor Highway on the Seward Peninsula, AK. Equipment for the experiments were driven to a staging location 70 m from the experimental plots and then hiked to the field sites on foot. Once constructed, NARS could be moved between the RFS plots. Water for simulations was acquired from the Kougarok River and Mauze Gulch.

the plots. Water for the experiments was pumped from the Kougarok River into a 568 L pillow tank located in a truck bed, which was then driven to the staging location 70 m from the RFS plots. The water was pumped from the pillow tank to the 1,893 L self-supporting tank. The flume was installed on the downslope edge of the RFS plot in a trench 200 cm × 60 cm × 60 cm. Water was directed from the RFS plot to the flume using a 200 cm long angle iron and a PVC guttering system (Figure 3). An additional 30 cm × 200 cm × 60 cm trench was excavated perpendicular to the main flume trench to allow water to drain from the flume and be bailed out. During simulations, one team member bailed water from the trench, two collected water samples, and two observed the simulator and sensor data.

3. RESULTS

3.1. NARS intensity and uniformity

In a single-frame module setup, using a single nozzle centered over the RFS plot, NARS had a maximum rain intensity of 50 mm/h with a uniformity of 79% over a 1.9 m × 1.45 m plot (Figure 5(a)). In a double-frame module setup, using two nozzles centered in each module, NARS had a maximum intensity of 82 mm/h with 73% uniformity over a 1.9 m × 2.9 m plot (Figure 5(b)). Increases in nozzle spacing resulted in a decrease in uniformity. Uniformity dropped to 55% when nozzles were spaced 101.6 cm from the center of the simulator and was 67% when the nozzles were spaced 127 cm from the center. Reducing the height of the nozzles prohibited the simulated rain from covering the full extent of the plot and produced an overlap in the spray pattern.

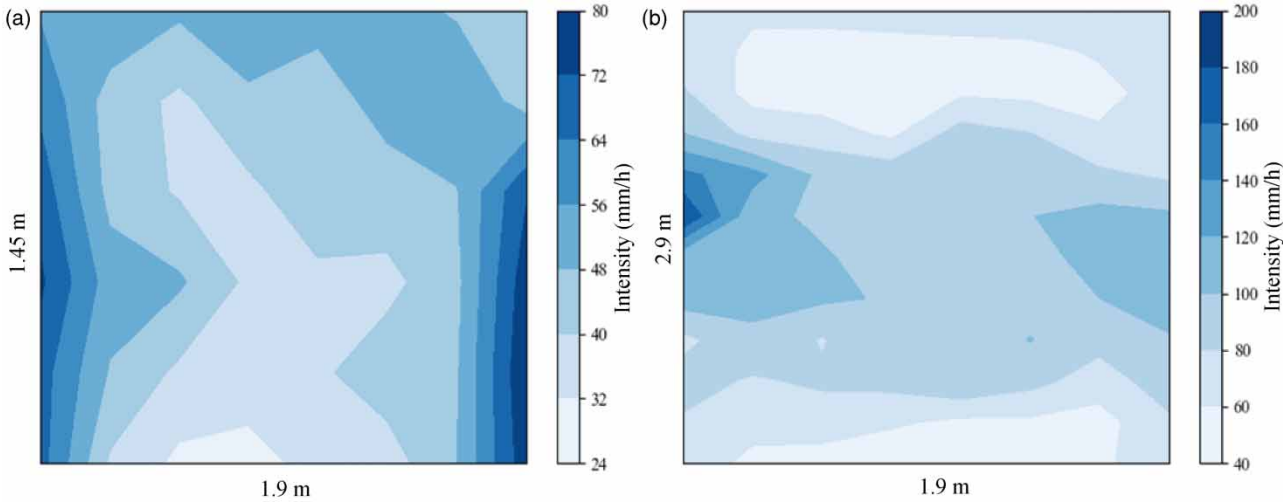

Figure 5 | Contour maps showing the relative intensity of the NARS. Deeper blues show areas that received more rainfall. (a) Rain intensity distribution in the single module setup using one nozzle centered over the 1.9 m × 1.45 m RFS plot. The average intensity over the plot was 50 mm/h with a uniformity of 79%. (b) Rain intensity distribution in the double module setup using two nozzles spaced 71.1 cm from the center of NARS, centering the nozzle over each respective module, on the 1.9 m × 1.45 m RFS plot. The average intensity over the plot was 82 mm/h with a uniformity of 73%.

3.2. eTape calibration and micro-HS-flume

The eTape had an activation depth of ~25 mm. Once above the detection limit, the eTape had a linear response to increases in water depth, and a sensitivity response of ~1 mm (Figure 6(a)). Initial discharge measurements were made with a commercially available 12.2 cm HS-flume (Figure 6(b)), which had a published measurement range from 4.5 to 2,274 mL/s with 2–5% accuracy (Brakensiek *et al.* 1979). The laboratory calibration of the eTape to the 12.2 cm HS-flume was performed from 0 to 118 mL/s, and the lowest discharge detected was 2.2 mL/s. However, the 12.2 cm HS-flume, which is the smallest commercially available HS-flume, lacked the sensitivity necessary to accurately capture the discharge generated by NARS (Figure 6(b)).

The two 3D-printed 4 cm micro-HS-flumes were able to capture the full range of expected NARS runoff generation. In our application, the maximum discharge possible using NARS is 122 mL/s, assuming all applied rainfall runs off the RFS plot. The micro-HS-flumes could handle maximum discharges of 150 mL/s (Figure 6(c)) and minimum discharge as low as 1.3 mL/s with high sensitivity for discharge changes. The 4 cm micro-HS-flume with the 0.64 cm × 0.64 cm opening to the stilling well had a rating curve response corresponding to the top of the stilling well opening (Supplementary Figure S5), where water height would not equilibrate between the stilling well and flume. The micro-HS-flume with the 1 cm × 3.6 cm opening to the stilling well had a consistent response, with water height remaining equal between the stilling well and flume.

3.3. NARS testing in the Arctic

The NARS's frame was bundled together into four groups of six aluminum frame pieces so that one team member could carry a bundle. Frame construction was accomplished by two people in ~1 h. NARS could then be easily moved between three different RFS plots by four field team members without deconstructing the frame.

Because of the distance from the experimental plot to the nearest river, there were logistical challenges in obtaining water for simulations. Additional logistical challenges included preparing the plot for discharge measurements, the electronics and sensors issues with moisture and measurement stabilization, and freezing conditions experienced during the deployment caused issues with the nozzle spray patterns and limited the ability to perform work in the mornings. However, despite these initial challenges, the experiments were only delayed to a later time during the day but were performed without negative impacts on the intensity and uniformity of simulated rainfall application to the plots. For more details on the challenges faced in the field deployment, see *Supplementary Material: Lessons Learned from the Arctic Deployment*.

Two rainfall experiments were performed that simulated an annual and a 1,000-year storm representative of the region, based on data from the nearest meteorological station, Quartz Creek (Station ID: 80-19080; 65.40673, −164.65703), which is ~5 km from the experimental plot and has provided continuous climate data since 1990. NOAA's Precipitation

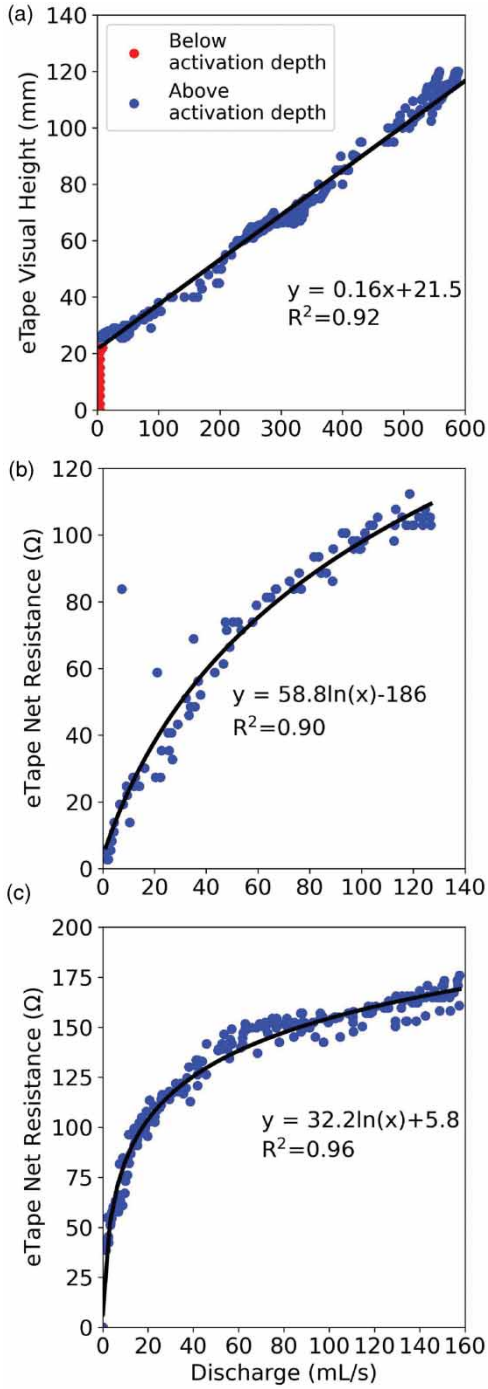

Figure 6 | Results from the eTape and HS-flume calibration experiments. (a) eTape calibration curve. The eTape had an activation depth of ~25 mm. Once above the activation depth, it had a linear response to changes in fluid level. The eTape could detect changes of ~1 mm fluid depth. (b) Commercially available 12.2 cm HS-Flume calibration curve. The 12.2 cm HS-Flume lacked the sensitivity necessary for the expected discharge range with the NARS. (c) 3D-printed 4 cm micro-HS-flume with the 1 cm × 3.6 cm opening to the stilling well. The smaller flume was able to fully capture the range of expected discharge while still having high sensitivity.

Frequency Data Server models recurrence intervals using Atlas 14 data and provides precipitation frequency estimates at 90% confidence. NARS delivered simulated rainfall at a controlled rate and the RPi collected interflow discharge data. The 4 cm 3D-printed micro-HS-flume was able to capture the full range of runoff, which peaked at 90 mL/s. Overall, NARS improves

upon RFS design to facilitate deployment in remote locations with its lightweight frame, water delivery design, and modern RFS controls.

4. DISCUSSION

4.1. NARS performance

4.1.1. Uniformity and intensity

There is a debate as to what is an adequate uniformity from RFSs. Some previous studies have suggested that specific uniformity criteria be met for rainfall simulation experiments, with coefficient of uniformity values of greater than 80–90% often cited as the criteria (Neff 1979; Keller & Bliesner 1990; Esteves *et al.* 2000; Iserloh *et al.* 2013; Green & Pattison 2022). Previously developed European RFSs have had uniformities ranging from 61 to 98% (Iserloh *et al.* 2013). What has perhaps been not fully appreciated is how the measured uniformity can change with different collection dish grid patterns, even if all other parameters remain the same. A higher density grid (e.g., 17 × 17) can yield a lower uniformity than a lower density grid (e.g., 8 × 8) due to the higher resolution grid highlighting local variation in the spray pattern (Green & Pattison 2022). Furthermore, modern computer simulations can account for different sections of the plot receiving more rainfall than others, decreasing the importance of high uniformity in the plot. In general, while a higher uniformity would be desirable under most foreseeable experimental conditions, we believe that RFSs with uniformity below 70% are still likely to be valuable research tools, provided uniformity is controlled and well defined. However, because of the extremely limited use of RFS in Arctic systems, this study and NARS provide a benchmark for use in such regions.

In our testing, NARS has a uniformity of 79% in a single-frame module setup and 73% in the double-frame module configuration. The decrease in the uniformity is caused by overlapping spray patterns produced by the two nozzles. Increasing the nozzle spacing leads to reduced uniformity, likely due to greater intensity differences between nonoverlapping and overlapping spray areas of the plot.

4.1.2. eTape and micro-HS-flume

The eTape's high sensitivity enables high-resolution measurement of changes in flume discharge, which made it ideal for our implementation. Instruments such as ultrasonic and pressure-depth sensors lack the resolution necessary to detect minor changes in flume level. Other similar water level sensors have issues with corrosion from exposed conductors or have calibration that changes due to water chemistry, which is resolved by the eTape's plastic casing.

Both of the 4 cm micro-HS-flumes are specially designed to capture the full range of runoff from NARS while maintaining high sensitivity at low discharge. The micro-HS-flume with the 1 cm × 3.6 cm stilling well opening provides a better response to changes in water levels in the flume compared to the micro-HS-flume with the 0.64 cm × 0.64 cm well opening because the water level between the flume and stilling well with the larger opening equilibrates more quickly. Although other simulators measure discharge by manually adjusting a variable resistor to match flume water height (Paige *et al.* 2004), recording a time lapse video to record height changes in a 5-gallon bucket (Schoener & Stone 2019), or taking discharge measurements using a graduated cylinder, the eTape allows for automated measurements of discharge. Manual measurement methods can introduce human error, lack resolution to observe discharge changes at low rates, do not account for particulates, and require at least one person to measure discharge.

The eTape and micro-HS-flume system provides automated high-resolution discharge measurements. However, to ensure accurate discharge measurements, the micro-HS-flume outlet must remain clear of any debris and must drain freely, and the eTape cannot be bent or jostled, without inducing errors in the measured resistance. Although commercially available flumes can cost thousands of dollars, the material to produce the 4 cm micro-HS-flumes cost ~$14.50 per flume, assuming a freely available 3D printer. The low-cost apparatus can also be applied in other remote settings, such as monitoring ephemeral streams, where installing commercial flumes can be cost prohibitive, and high discharge resolution at low-flow regimes is a key.

4.2. Summary of NARS improvements and limitations

NARS improves upon previous RFS designs to facilitate RFS deployment in remote field locations in the Arctic in the following ways:

1. *The use of a lightweight and modular frame design*. The frame design requires few tools to assemble and can be fully deconstructed, improving its transportability to isolated field locations. In addition, the modular frame design can be used to create a larger study plot size without completely redesigning the simulator.
2. *Updates to water delivery methods.* The fixed water conduit eliminates the need for a motor to rotate the boom, simplifies RFS design, reduces the number of components that can fail, and decreases the total weight of the simulator. The threaded unions used to join the PVC water conduit will be replaced with cam-and-groove fittings, which are easier to join. The use of garden hoses rather than 5.08 cm discharge hose drastically reduces the total weight of the water system. Rather than rigid agriculture water tanks, the collapsible water tanks are lightweight and foldable, which allows one person to carry them to field sites.
3. *Modernization RFS controls with a* RPi *microcomputer.* The RPi controls NARS and acquires data in one system rather than requiring a computer with an external data logger. The RPi is controlled through a GUI and requires no programming to operate and readily integrates with a variety of sensors, further expanding its adaptability.
4. *The development of a micro-HS-flume to capture discharge*. Discharge measurements are automated with the eTape sensor and provide greater low flow regime accuracy than other methods. 3D printing the micro-HS-flume is inexpensive, and the resultant flumes can be tailored to fit a variety of applications.

Though NARS is an improvement in previous RFS designs for remote deployment, NARS field deployments can be further improved in the following ways:

1. *Water transportation to the field site*. Pumps with higher flow rate that are better at pumping water uphill would be a better option than the electric pumps used for staging water for experiments.
2. *Trench emplacement*. The flume trench size could be reduced by using a small submersible pump to remove water from the trench rather than manually bailing water from the trench.
3. *Sensors*. The threaded thermocouple will be replaced with a thermocouple that is attached to NARS using a compression fitting, which will enable the thermocouple to be removed from NARS without rotating the sensor itself, reducing the risk of fraying the wires. The eTape was the best sensor option for measurement of flume depth; however, the eTape sensors are sensitive and cannot be bent or shifted during an experiment, without suffering a loss in accuracy.
4. *Control box*. NARS intensity and data collection controls will be separated into two control boxes. The control boxes will be self-contained so that the electronics and sensors are protected from water and the weather.
5. *Team size*. A six-member team that could be split into three teams of two would be beneficial for field deployments and would allow frame construction, water staging, and flume emplacement to be accomplished concurrently.

4.3. Future applications of NARS

NARS is a novel tool for studying rainfall effects in the Arctic. The design of NARS improves on previous RFSs to facilitate deployment in remote field locations, and unlike RFSs previously used in the Arctic (Magnússon *et al.* 2022), NARS is capable of variable rainfall supplication rates and intensities. As rainfall frequency and intensity are expected to increase in the Arctic (Dou *et al.* 2022), experiments derived from NARS deployments can be used to predict the impact of future storms on permafrost stability. For example, the simulator can be used to experimentally study the effects of seasonal changes in rainfall timing, duration, and intensity on thermal, hydrologic, and chemical fluxes through permafrost soils at various states of thaw. In addition, repeated measurements of active layer thickness within experimental plots and control plots throughout many field seasons and throughout multiple applications at various simulated rainfall rates and intensities will aid in assessing the impacts of rainfall on permafrost stability in controlled and repeatable experiments. The Micro-HS-flume allows for water samples to be collected from the experimental plot during and after the experiment, so that the impacts of increased rainfall on soil water geochemistry can be assessed. However, as indicted in the lessons learned from the logistical challenges faced during field deployment, proximity to a continuous water source such as a river or lake is essential for performing numerous experiments in Arctic regions.

5. CONCLUSIONS

The NARS is a variable intensity RFS that combines aspects of previous RFSs to create a simulator that is better suited for deployment in the Arctic and other isolated environments through:

- A lightweight aluminum frame that can be easily carried into remote locations
- Novel HS-Flumes for high-resolution discharge measurement
- Modernization of simulator controls and data collection using a RPi

As the frequency and intensity of rainfall is expected to increase in the Arctic, NARS is a unique tool that can be used to study the effects that changing rainfall patterns have on permafrost processes at the plot scale. Knowledge gained from NARS experiments will provide a better understanding of rain effects on permafrost, enabling better predictions on rates of permafrost thaw and carbon release as the Arctic warms.

ACKNOWLEDGEMENTS

Funding for this research was provided by the Department of Energy Office of Science, Office of Biological and Environmental Research through NGEE Arctic project. We would like to thank Ginger Paige for allowing us to use the Walnut Gulch Rainfall Simulator, which allowed us to study rainfall simulator design and experimental techniques.

DATA AVAILABILITY STATEMENT

Data are available on the NGEE Arctic Data portal at https://doi.org/10.5440/1960551 and https://doi.org/10.5440/1960549.

CONFLICT OF INTEREST

The authors declare there is no conflict.

REFERENCES

Agassi, M. & Bradford, J. M. 1999 Methodologies for interrill soil erosion studies. *Soil and Tillage Research* **49**, 277–287. https://doi.org/10.1016/S0167-1987(98)00182-2.

Akhter, F., McMain, J. T., McLemore, A. J. & Hurst, M. J. 2021 Validation and development of discharge equations for 3D printed flumes for flow monitoring. *Transactions of the ASABE* **64**, 1921–1928. https://doi.org/doi: 10.13031/trans.14365.

Beutner, E. L., Gaebe, R. R. & Horton, R. E. 1940 Sprinkled-plan runoff- and infiltration-experiments on desert-soils. *Eos, Transactions American Geophysical Union* **21**, 550–558. https://doi.org/10.1029/TR021i002p00550.

Bintanja, R. & Selten, F. M. 2014 Future increases in Arctic precipitation linked to local evaporation and sea-ice retreat. *Nature* **509**, 479–482. https://doi.org/10.1038/nature13259.

Bowden, W. B., Gooseff, M. N., Balser, A., Green, A., Peterson, B. J. & Bradford, J. 2008 Sediment and nutrient delivery from thermokarst features in the foothills of the North Slope, Alaska: Potential impacts on headwater stream ecosystems. *Journal of Geophysical Research* **113**. https://doi.org/10.1029/2007JG000470.

Brakensiek, D. L., Osborn, H. & Rawls, W. 1979 Field manual for research in agricultural hydrology. In: *Agriculture Handbook No 224* (Brakensiek, D. L., Osborn, H. B. & Rawls, W. J., eds.). United Department of Agriculture, Washington, DC.

Christiansen, J. E. 1940 Irrigation by sprinkling. University of California Agriculture Experiments Station Bulletin 670.

Domine, F., Fourteau, K., Picard, G., Lackner, G., Sarrazin, D. & Poirier, M. 2022 Permafrost cooled in winter by thermal bridging through snow-covered shrub branches. *Nature Geoscience* **15**, 554–560. https://doi.org/10.1038/s41561-022-00979-2.

Dou, T. F., Pan, S. F., Bintanja, R. & Xiao, C. D. 2022 More frequent, intense, and extensive rainfall events in a strongly warming Arctic. *Earth's Future* **10**, e2021EF002378. https://doi.org/10.1029/2021EF002378.

Douglas, T. A., Turetsky, M. R. & Koven, C. D. 2020 Increased rainfall stimulates permafrost thaw across a variety of Interior Alaskan boreal ecosystems. *npj Climate and Atmospheric Science* **3**, 28. https://doi.org/10.1038/s41612-020-0130-4.

Esteves, M., Faucher, X., Galle, S. & Vauclin, M. 2000 Overland flow and infiltration modelling for small plots during unsteady rain: numerical results versus observed values. *Journal of Hydrology* **228** (3–4), 265–282.

Free, G. R., Browning, G. M. & Musgrave, G. W. 1940 Relative Infiltration and Related Physical Characteristics of Certain Soils. Technical Bulletin No 729 55.

Green, D. & Pattison, I. 2022 Christiansen uniformity revisited: Re-thinking uniformity assessment in rainfall simulator studies. *Catena* **217**, 106424. https://doi.org/10.1016/j.catena.2022.106424.

Grünberg, I., Wilcox, E.J., Zwieback, S., Marsh, P. & Boike, J. 2020 Linking tundra vegetation, snow, soil temperature, and permafrost. *Biogeosciences* **17**, 4261–4279. https://doi.org/10.5194/bg-17-4261-2020.

Gwinn, W. 1984 Chute entrances for HS, H, and HL flumes. *Journal of Hydraulic Engineering* **110**, 5.

Gwinn, W. & Parsons, D. 1976 Discharge equations for HS, H, and HL flumes. *Journal of the Hydraulics Division* **102** (1), 73–88.

Humphry, J. B., Daniel, T. C., Edwards, D. R. & Sharpley, A. N. 2002 A portable rainfall simulator for plot-scale runoff studies. *Applied Engineering in Agriculture* **18** (2), 199. https://doi.org/10.13031/2013.7789.

Iijima, Y., Fedorov, A. N., Park, H., Suzuki, K., Yabuki, H., Maximov, T. C. & Ohata, T. 2010 Abrupt increases in soil temperatures following increased precipitation in a permafrost region, central Lena River basin, Russia: Abrupt soil warming in Eastern Siberia. *Permafrost Periglac Process* **21**, 30–41. https://doi.org/10.1002/ppp.662.

Iserloh, T., Ries, J. B., Arnáez, J., Boix-Fayos, C., Butzen, V., Cerdà, A., Echeverría, M. T., Fernández-Gálvez, J., Fister, W., Geißler, C. & Gómez, J. A. 2013 European small portable rainfall simulators: A comparison of rainfall characteristics. *CATENA* **110**, 100–112. https://doi.org/10.1016/j.catena.2013.05.013.

Jorgenson, M. T., Romanovsky, V., Harden, J., Shur, Y., O'Donnell, J., Schuur, E. A., Kanevskiy, M. & Marchenko, S. 2010 Resilience and vulnerability of permafrost to climate change. *Canadian Journal of Forest Research* **40**, 18.

Keller, J. & Bliesner, R. 1990 *Sprinkler and Trickle Irrigation*. Van Nostrand Reinhold, New York.

Lafrenière, M. J. & Lamoureux, S. F. 2019 Effects of changing permafrost conditions on hydrological processes and fluvial fluxes. *Earth-Science Reviews* **191**, 212–223. https://doi.org/10.1016/j.earscirev.2019.02.018.

Li, L., Nearing, M. A., Polyakov, V. O., Nichols, M. H., Pierson, F. B. & Cavanaugh, M. L. 2020 Evolution of rock cover, surface roughness, and its effect on soil erosion under simulated rainfall. *Geoderma* **379**, 114622. https://doi.org/10.1016/j.geoderma.2020.114622.

Liljedahl, A., Hinzman, L., Busey, R. & Yoshikawa, K. 2007 Physical short-term changes after a tussock tundra fire, Seward Peninsula, Alaska. *Journal of Geophysical Research* **112**, F02S07. https://doi.org/10.1029/2006JF000554.

Lindgren, A., Hugelius, G. & Kuhry, P. 2018 Extensive loss of past permafrost carbon but a net accumulation into present-day soils. *Nature* **560**, 219–222. https://doi.org/10.1038/s41586-018-0371-0.

Magnússon, R. Í., Hamm, A., Karsanaev, S. V., Limpens, J., Kleijn, D., Frampton, A., Maximov, T. C. & Heijmans, M. M. 2022 Extremely wet summer events enhance permafrost thaw for multiple years in Siberian tundra. *Nature Communications* **13**, 1556. https://doi.org/10.1038/s41467-022-29248-x.

Marr, J., Johns, S. & Busch, D. 2010 Performance Assessment of H Flumes Under Extreme Approach Flow Conditions. St. Anthony Falls Laboratory. Project Reports 538.

McCrystall, M. R., Stroeve, J., Serreze, M., Forbes, B. C. & Screen, J. A. 2021 New climate models reveal faster and larger increases in Arctic precipitation than previously projected. *Nature Communications* **12**, 6765. https://doi.org/10.1038/s41467-021-27031-y.

Meyer, L. D. & Harmon, W. C. 1979 Multiple-Intensity rainfall simulator for erosion research on row sideslopes. *Transactions of the ASAE* **22** (1), 100–103.

Miner, K. R., Turetsky, M. R., Malina, E., Bartsch, A., Tamminen, J., McGuire, A. D., Fix, A., Sweeney, C., Elder, C. D. & Miller, C. E. 2022 Permafrost carbon emissions in a changing Arctic. *Nature Reviews Earth and Environment* **3**, 55–67. https://doi.org/10.1038/s43017-021-00230-3.

Myers-Smith, I. H. & Hik, D. S. 2013 Shrub canopies influence soil temperatures but not nutrient dynamics: An experimental test of tundra snow-shrub interactions. *Ecology and Evolution* **3**, 3683–3700. https://doi.org/10.1002/ece3.710.

Neff, E. L. 1979 March. Why rainfall simulation. In *Proceedings of rainfall simulator workshop*, Tucson, AZ, 7-9 March 1979. USDA-SEA ARM-W-10, pp. 3–7.

Obu, J. 2021 How much of the earth's surface is underlain by permafrost? *JGR Earth Surface* **126**. https://doi.org/10.1029/2021JF006123.

Olefeldt, D., Goswami, S., Grosse, G., Hayes, D., Hugelius, G., Kuhry, P., McGuire, A. D., Romanovsky, V. E., Sannel, A. B. K., Schuur, E. A. G. & Turetsky, M. R. 2016 Circumpolar distribution and carbon storage of thermokarst landscapes. *Nature Communications* **7**, 13043. https://doi.org/10.1038/ncomms13043.

Paige, G. B., Stone, J. J., Smith, J. R. & Kennedy, J. R. 2004 The Walnut Gulch Rainfall Simulator: A computer-controlled variable intensity rainfall simulator. *Applied Engineering in Agriculture* **20**, 25–31. https://doi.org/10.13031/2013.15691.

Pierson, F. B., Moffet, C. A., Williams, C. J., Hardegree, S. P. & Clark, P. E. 2009 Prescribed-fire effects on rill and interrill runoff and erosion in a mountainous sagebrush landscape. *Earth Surf Process Landforms* **34**, 193–203. https://doi.org/10.1002/esp.1703.

Polyakov, V., Stone, J., Holifield Collins, C., Nearing, M. A., Paige, G., Buono, J. & Gomez-Pond, R. L. 2018 Rainfall simulation experiments in the southwestern USA using the Walnut Gulch Rainfall Simulator. *Earth System Science Data* **10** (1), 19–26.

Quinton, J. N., Edwards, G. M. & Morgan, R. P. C. 1997 The influence of vegetation species and plant properties on runoff and soil erosion: Results from a rainfall simulation study in southeast Spain. *Soil Use & Management* **13**, 143–148. https://doi.org/10.1111/j.1475-2743.1997.tb00575.x.

Schindewolf, M. & Schmidt, J. 2012 Parameterization of the EROSION 2D/3D soil erosion model using a small-scale rainfall simulator and upstream runoff simulation. *CATENA* **91**, 47–55. https://doi.org/10.1016/j.catena.2011.01.007.

Schoener, G. & Stone, M. C. 2019 Impact of antecedent soil moisture on runoff from a semiarid catchment. *Journal of Hydrology* **569**, 627–636. https://doi.org/10.1016/j.jhydrol.2018.12.025.

Schuur, E. A., McGuire, A. D., Schädel, C., Grosse, G., Harden, J. W., Hayes, D. J., Hugelius, G., Koven, C. D., Kuhry, P., Lawrence, D. M. & Natali, S. M. 2015 Climate change and the permafrost carbon feedback. *Nature* **520**, 171–179. https://doi.org/10.1038/nature14338.

Singh, S. P., Tack, F. M. G., Gabriels, D. & Verloo, M. G. 2000 Heavy metal transport from dredged sediment derived surface soils in a laboratory rainfall simulation experiment. *Water, Air, and Soil Pollution* **118**, 73–86.

Sturm, M., Holmgren, J., McFadden, J. P., Liston, G. E., Chapin, F. S. & Racine, C. H. 2001 Snow–shrub interactions in Arctic tundra: A hypothesis with climatic implications. *Journal of Climate* **14**, 336–344. https://doi.org/10.1175/1520-0442(2001)014 < 0336:SSIIAT > 2.0.CO;2.

Sulman, B. N., Salmon, V. G., Iversen, C. M., Breen, A. L., Yuan, F. & Thornton, P. E. 2021 Integrating Arctic plant functional types in a land surface model using above- and belowground field observations. *Journal of Advances in Modeling Earth Systems* **13**. https://doi.org/10.1029/2020MS00296.

Tossell, R. W., Dickinson, W. T. & Wall, G. J. 1987 A portable rainfall simulator. *Canadian Agricultural Engineering* **29** (2), 155–162.

First received 5 September 2023; accepted in revised form 14 November 2023. Available online 8 December 2023